Journal of Molecular Modeling (2018) 24:296
https://doi.org/10.1007/s00894-018-3828-z

ORIGINAL PAPER

Cage-like $B_{40}C_{30}$, $B_{40}C_{40}$, and $B_{40}C_{50}$: high-symmetry heterofullerenes isovalent with C_{60}, C_{70}, and C_{80}

Miao Yan[1] · Xin-Xin Tian[1] · Ling Pei[1] · Si-Dian Li[1]

Received: 15 February 2018 / Accepted: 12 September 2018

Abstract

The recent discovery of the cage-like borospherenes $B_{40}^{-/0}$, composed of interwoven double chains of boron, presents the possibility of forming B_mC_n heterofullerenes as hybrids of borospherenes and carbon fullerenes in dual spaces. Based on extensive first-principles theory calculations, we predict herein the possible existence of the high-symmetry B_mC_n heterofullerenes S_{10} $B_{40}C_{30}$ (**1**), C_5 $B_{40}C_{40}$ (**2**), and S_{10} $B_{40}C_{50}$ (**3**), which are isovalent with C_{60}, C_{70}, and C_{80}, respectively. These beautiful borafullerenes with boron aggregations feature one B_{30} boron double-chain nanoring at the equator, two bowl-shaped C_{15} or C_{25} caps at the top and bottom, and ten quasi-planar tetracoordinate peripheral C atoms in ten B-centered B_6C hexagonal pyramids that are evenly distributed around the waist in a seamless "patched" structural motif. Detailed orbital and bonding analyses indicate that, as they are isovalent with C_{60}, C_{70}, and C_{80}, respectively, $B_{40}C_{30}$ (**1**), $B_{40}C_{40}$ (**2**), and $B_{40}C_{50}$ (**3**) possess 30, 35, and 40 π bonds, respectively, of which 20 are 5c-2e π bonds delocalized over ten hexagonal pyramids that are evenly distributed around the waist. Such structural and bonding patterns confer high stability to these B-C heterofullerenes, which may be synthesized in experiments.

Keywords Heterofullerenes · Borafullerenes · First-principles theory calculations · Structures · Bonding analyses

Introduction

C_{60} and C_{70} fullerenes have been superstars in chemistry and materials science ever since their discovery in 1985 [1] and isolation in 1990 [2, 3]. The band gaps E_g of C_{60} and C_{70} powders were experimentally measured to be 1.86 and 1.57 eV, respectively [4]. Given the similarity between boron and carbon in both atomic size and chemical bonding, it is perhaps not surprising that boron-doped fullerenes with one or more of the carbon atoms of the fullerene substituted by boron were first observed in the gas phase in 1991 [5] (i.e., soon after the first isolation of pure carbon fullerenes), and were first extracted from doped carbon soot in 1996 [6]. Theoretical investigations of the geometric and electronic structures of B-C binary clusters such as $C_{59}B$, $C_{69}B$, $C_{60-n}B_n$ (n = 1–12), and $C_{12}B_{68}$ have also been reported in the literature [7–10]. Mohr and coworkers recently performed an extensive global search for cage-like $B_{12}C_{48}$ and $B_{12}C_{50}$ clusters using the minimum hopping method (MH) and found that "patched" motifs with boron aggregations around two neighboring B-centered B_5C_2 hexagonal pyramids were much more stable than the previously reported "diluted" structures [11]. The experimental formation of heterofullerenes $B_{59}C^-$ and $B_{69}C^-$ in 2013 by directly exposing C_{60} and C_{70} to boron vapor paves the way to the production of borafullerenes in macroscopic quantities through atom exchange [12]. All-boron fullerenes were not considered until the proposal of the cage-like B_{80} in 2007, which was constructed by capping the 20 hexagons in C_{60} [13], though subsequent density functional theory (DFT) investigations showed that core–shell structures are much lower in energy [14, 15]. The first all-boron fullerenes, $B_{40}^{-/0}$, dubbed borospherenes, were discovered in the gas phase in a joint experimental and theoretical investigation in 2014 [16]. The electronic structures and electronic spectra of neutral B_{40} were computationally simulated

Electronic supplementary material The online version of this article (https://doi.org/10.1007/s00894-018-3828-z) contains supplementary material, which is available to authorized users.

✉ Xin-Xin Tian
tianxx@sxu.edu.cn

✉ Si-Dian Li
lisidian@sxu.edu.cn

[1] Institute of Molecular Science, Shanxi University, Taiyuan 030006, Shanxi, People's Republic of China

Published online: 25 September 2018

shortly after [17]. An axially chiral borospherene, B_{39}^-, was observed late in 2015 [18]. Our group have extended the borospherene family explored at the first-principles theory level in the past 3 years to include the B_n^q series ($q = n - 40$, $n = 36$–42), all of which are composed of 12 interwoven double chains of boron with six hexagonal or heptagonal faces on the cage surface and follow the universal σ + π double delocalization bonding pattern [19–22]. The seashell-like $B_{28}^{-/0}$ and B_{29}^- borospherenes have also been observed as minor isomers in the gas phase [23, 24]. The establishment of the borospherene family presents the possibility of forming cage-like B_mC_n heterofullerenes with high boron contents ($m \approx n$) as hybrids of borospherenes and carbon fullerenes in dual spaces. Boron double chains (BDCs) may thus be patched into carbon fullerenes in seamless motifs. However, to the best of our knowledge, no such cage-like B_mC_n borafullerenes with high boron contents ($m \approx n$) that have structural characteristics of both borospherenes and carbon fullerenes have been reported from either experimental or theoretical studies.

Based on extensive first-principles theory calculations, we explore herein the possibility of generating the cage-like B-C binary fullerenes with high boron contents S_{10} $B_{40}C_{30}$ (**1**), C_5 $B_{40}C_{40}$ (**2**), and S_{10} $B_{40}C_{50}$ (**3**), which are isovalent with C_{60}, C_{70}, and C_{80}, respectively. These borafullerenes with boron aggregations feature a B_{30} BDC nanoring at the equator, two bowl-shaped C_{15} or C_{25} caps at the top and bottom, and ten quasi-planar tetracoordinate pyramids around the waist. They all possess 20 5c-2e π-bonds delocalized over ten hexagonal pyramids evenly distributed along the B_{30} double-chain nanoring. The IR, Raman, and UV-vis spectra of $B_{40}C_{30}$ (**1**) were computationally simulated to facilitate its spectroscopic characterization.

Methods

Initial high-symmetry structures of $B_{40}C_{30}$, $B_{40}C_{40}$, and $B_{40}C_{50}$ were manually constructed utilizing chemical intuition from their isovalent fullerene counterparts I_h C_{60}, D_{5h} C_{70}, and D_{5d} C_{80}, respectively. Extensive global searches were performed on $B_{40}C_{30}$ using both the constrained basin-hopping algorithm implemented in the TGMin program [25, 26] and the minima hopping (MH) method [27, 28], which yields the global minimum configuration as well as many other low-energy metastable structures at the PBE level and probes over 7500 stationary points on the potential energy surface. The low-lying isomers thus obtained were then fully re-optimized at the hybridized DFT-PBE0 level with the 6-31G* and 6–311 + G* basis sets [29, 30]. The hybridized PBE0 functional provides reliable results for boron-based nanoclusters with a wide range of sizes, according to comparisons with experimental data or the results afforded by more accurate ab initio calculations [16–24]. No global searches were executed on the more complicated $B_{40}C_{40}$ and $B_{40}C_{50}$ systems due to the limitations of the available computing resources. Frequency checks were performed at the PBE0/6-31G* level to ensure that all of the low-lying structures obtained were true minima of the systems of interest. Detailed bonding analyses were performed using the adaptive natural density partitioning (AdNDP) [31–33] method at the PBE0/6-31G level, and the results were visualized using the Molekel 5.4.0.8 program [34]. All calculations performed in this work were implemented using the Gaussian 09 package [35].

Results and discussion

Structures and stabilities

We first consider $B_{40}C_{30}$, the first and most important B-C binary cluster of interest in this work. This cluster is isovalent with the best-known fullerene, C_{60} [1, 2], with 240 valence electrons in peripheral C atoms in ten B-centered B_6C hexagonals. S_{10} $B_{40}C_{30}$ (**1**), the high-symmetry isomer that exhibits a "patched" motif in which 40 boron atoms are aggregated into ten B-centered B_6C hexagonal pyramids evenly distributed around the waist, was found to be the most stable structure (Fig. 1 and Fig. S1 in the "Electronic supplementary material," ESM). However, given its extremely complicated potential energy surface, we cannot guarantee that the true

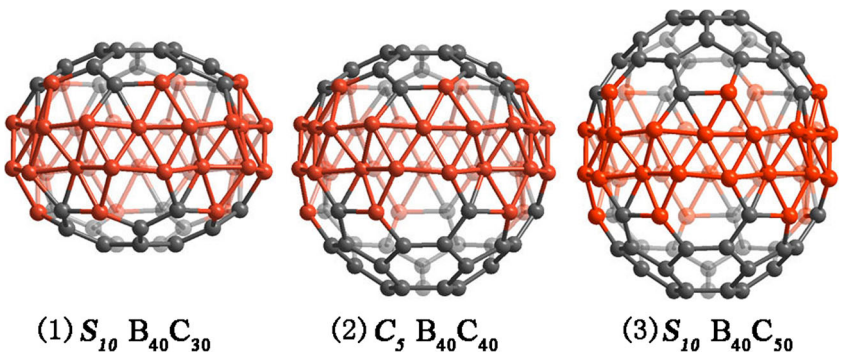

Fig. 1 Optimized structures of S_{10} $B_{40}C_{30}$ (**1**), C_5 $B_{40}C_{40}$ (**2**), and S_{10} $B_{40}C_{50}$(**3**), as calculated at the PBE0/6–311 + G* level

global minimum of the binary system was located. $B_{40}C_{30}$ (**1**) possesses obvious similarity with the global minimum of $B_{48}C_{12}$, which contains two neighboring B-centered B_5C_2 hexagonal pyramids obtained via MH global searches [11]. It features one B_{30} BDC nanoring at the equator, two eclipsed bowl-shaped C_{15} caps at the top and bottom, and ten quasi-planar tetracoordinate peripheral C atoms in ten B-centered B_6C hexagonal pyramids that are evenly distributed around the waist in a seamless patched motif with an overall symmetry of S_{10}. This appears to be 0.23 eV more stable than the second lowest-lying isomer, C_1 $B_{40}C_{30}$, which also contains a B_{30} boron double-chain nanoring at the equator and two bowl-shaped C_{15} caps at the top and bottom in C_1 symmetry (Fig. S1 in the ESM). The third isomer, C_1 $B_{40}C_{30}$, has one C_{20} cap at the top, one C_{10} cap at the bottom, and one distorted B_{40} belt between the two carbon caps, and is 0.42 eV less stable than S_{10} $B_{40}C_{30}$ (**1**). Other isomers were found to be much less stable than $B_{40}C_{30}$ (**1**), as their energies were at least 0.94 eV higher. Core–shell structures were found to be highly unstable, with relative energies of greater than +8.0 eV (Fig. S1 in the ESM). There is not much to choose between cage-like $B_{40}C_{30}$ isomers with boron aggregations [10] in terms of stability to satisfy the bonding requirements of both carbon and boron: it is known from experiments that carbon favors peripheral positions in B-C binary clusters such as CB_8^-, $C_2B_8^-$, and CB_9^-, while boron may serve as penta- or hexacoordinate centers to compensate for the electron deficiency in boron-rich areas [36, 37]. S_{10} $B_{40}C_{30}$ (**1**), with one B_{30} BDC nanoring around the waist and two equivalent C_{15} caps at the top and bottom (which may be better formulated as S_{10} $C_{15}B_{40}C_{15}$), best matches the bonding requirements of the boron and carbon atoms in the binary system. Specific σ- and π-bonding patterns will be discussed later.

Following the structural pattern of S_{10} $B_{40}C_{30}$ (**1**), and noting the known structures of D_{5h} C_{70} and D_{5d} C_{80}, we manually constructed the high-symmetry C_5 $B_{40}C_{40}$ (**2**) and S_{10} $B_{40}C_{50}$ (**3**) with 40 B atoms aggregated in ten B-centered B_6C hexagonal pyramids that are evenly distributed around the waist (Fig. 1). Both $B_{40}C_{40}$ (**2**) and $B_{40}C_{50}$ (**3**) contain a B_{30} BDC nanoring at the equator, with the former containing one bowl-shaped C_{15} cap at the top and one C_{25} cap at the bottom (which can be formulated as C_5 $C_{15}B_{40}C_{25}$), whereas the latter possesses two eclipsed C_{25} caps at the top and bottom of the elongated cage (i.e., S_{10} $C_{25}B_{40}C_{25}$). Such cage-like motifs with a BDC nanoring patched seamlessly into the fullerene framework provide the optimum geometry to satisfy the bonding requirements of B_mC_n binary clusters with high boron contents.

Electronic structures and bonding analyses

The high stabilities of the $B_{40}C_n$ series (n = 30, 40, 50) originate from their unique electronic structures and bonding patterns. Figure 2 presents the molecular orbital energy level diagrams of S_{10} $B_{40}C_{30}$ (**1**), C_5 $B_{40}C_{40}$ (**2**), and S_{10} $B_{40}C_{50}$ (**3**), as calculated at the PBE0/6–311 + G* level, with their HOMO and LUMO distributions and HOMO–LUMO energy gaps indicated. These heterofullerenes possess large HOMO–LUMO energy gaps of ΔE_{gap} = 2.65, 2.89, and 2.64 eV when calculated at the PBE0/6–311 + G* level, respectively, which are comparable with the corresponding values of 2.99, 2.93, 3.13, and 2.89 eV computed for I_h C_{60}, D_{5h} C_{70}, D_{2d} B_{40} [16], and C_3 B_{39}^- [18] at the same theoretical level, thus supporting the notion that these $B_{40}C_n$ binary clusters (n = 30, 40, and 50) with closed-shell electronic configurations have high chemical stabilities. Interestingly, the HOMO–LUMO gap of $B_{40}C_{50}$ (**3**) appears to be even wider than that (1.15 eV) of D_{5d} C_{80} at the PBE0 level. As shown in Fig. 2, the HOMOs of these heterofullerenes are all bonding orbitals, whereas their LUMOs are antibonding, in line with the large HOMO–LUMO energy gaps for these binary clusters. We also notice that the five degenerate HOMO (h_u) orbitals of I_h C_{60} are broken into one nondegenerate orbital (a_u) and two sets of doubly degenerate orbitals in $B_{40}C_{30}$ (**1**). The same is true of $B_{40}C_{40}$ (**2**) and $B_{40}C_{50}$ (**3**) (Fig. 2). It is worth mentioning that the previously predicted fullerene-like clusters $C_{36}B_{24}$, $C_{24}B_{36}$, and $C_{36}N_{24}$, which are not isovalent with C_{60}, present much narrower HOMO–LUMO gaps than C_{60} [38].

AdNDP analyses revealed both the localized and delocalized chemical bonds in the systems. As shown in Fig. 3a, there are 90 2c-2e C–C σ bonds with occupation numbers |ON| of 1.97–1.99 |e| and 30 2c-2e C–C π bonds with |ON| = 1.64 |e| in I_h C_{60}, fully satisfying the sp^2 bonding requirements of the 60 C atoms. A similar bonding pattern is present in S_{10} $B_{40}C_{30}$ (**1**), which possesses 40 2c-2e σ bonds at the top and bottom with |ON| = 1.93–1.98 |e|, 40 3c-2e σ bonds in 40 triangles around the waist with |ON| = 1.95 |e|, and ten 4c-2e σ bonds in ten B_4 rhombuses between the ten neighboring B_6C hexagonal pyramids with |ON| = 1.91 |e|. The remaining 30 π bonds can be classified into two sets: ten 2c-2e C–C π bonds in the two C_{15} caps with |ON| = 1.67 |e| and 20 5c-2e π bonds evenly distributed over the ten B-centered B_6C hexagonal pyramids along the B_{30} boron double-chain nanoring with |ON| = 1.67–1.74 |e|. These σ- and π-bonding patterns show a one-to-one correspondence with those of C_{60} (Fig. 3a), and confer high stability to $B_{40}C_{30}$ (**1**).

Similar σ- and π-bonding patterns were obtained for both C_5 $B_{40}C_{40}$ (**2**) and S_{10} $B_{40}C_{50}$ (**3**). As shown in Fig. 3b, C_5 $B_{40}C_{40}$ (**2**) possesses a σ skeleton with 55 2c-2e σ bonds, 40 3c-2e σ bonds, and ten 4c-2e σ bonds on the cage surface. Its π system includes 15 2c-2e π bonds in the C_{15} cap at the top and the C_{25} cap at the bottom, and 20 5c-2e π bonds in the ten B-centered hexagonal pyramids around the waist. Both the σ- and π-bonding patterns of C_5 $B_{40}C_{40}$ (**2**) appear to be similar to those of D_{5h} C_{70} (Fig. 3b and Fig. S2 in the ESM). S_{10} $B_{40}C_{50}$ (**3**), the largest heterofullerene studied in this work,

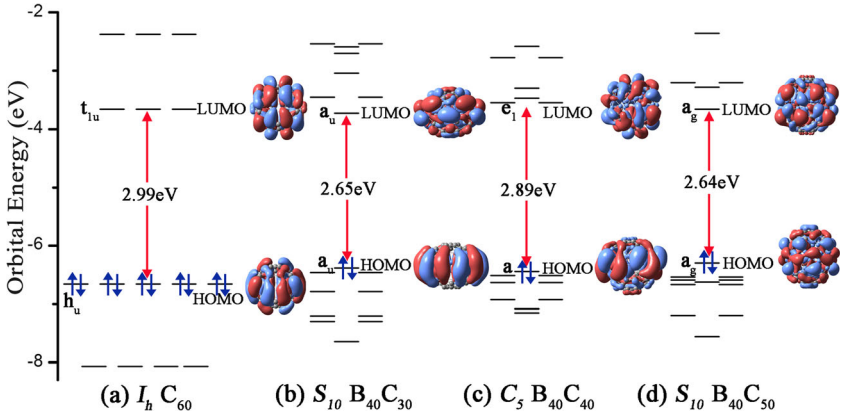

Fig. 2a–d Molecular orbital energy diagrams near the HOMOs and LUMOs of **a** I_h C_{60}, **b** S_{10} $B_{40}C_{30}$ (**1**), **c** C_5 $B_{40}C_{40}$ (**2**), and **d** S_{10} $B_{40}C_{50}$ (**3**), as calculated at the PBE0/6–311 + G* level, with HOMO occupation indicated by *arrows*

contains 70 2c-2e σ bonds, 40 3c-2e σ bonds, and ten 4c-2e σ bonds on the cage surface, 20 2c-2e π bonds in the two C_{25} caps, and 20 5c-2e π bonds in the ten B_6C hexagonal pyramids around the waist—again, similar to the fullerene D_{5d} C_{80} (Fig. 3c and Fig. S2 in the ESM). It is noticeable that $B_{40}C_{30}$ (**1**), $B_{40}C_{40}$ (**2**), and $B_{40}C_{50}$ (**3**) all possess 20 5c-2e π-bonds in ten B-centered B_6C hexagonal pyramids that are evenly distributed around the waist. Such bonding patterns grant 3D spherical aromaticity to the cage-like $B_{40}C_n$ binary fullerenes (n = 30, 40, and 50), as evidenced by the negative values (−15, −24, and − 20 ppm) of the calculated nucleus-independent chemical shifts (NICSs) [39] at the cage centers of $B_{40}C_{30}$ (**1**), $B_{40}C_{40}$ (**2**), and $B_{40}C_{50}$ (**3**), respectively.

Simulated IR, Raman, and UV-vis spectra

The infrared (IR), Raman, and UV-vis spectra of $B_{40}C_{30}$ (**1**) were computationally simulated to facilitate its spectral characterization (Fig. 4). Similar spectroscopic simulations have previously been reported for B_{40} [17]. Infrared photodissociation

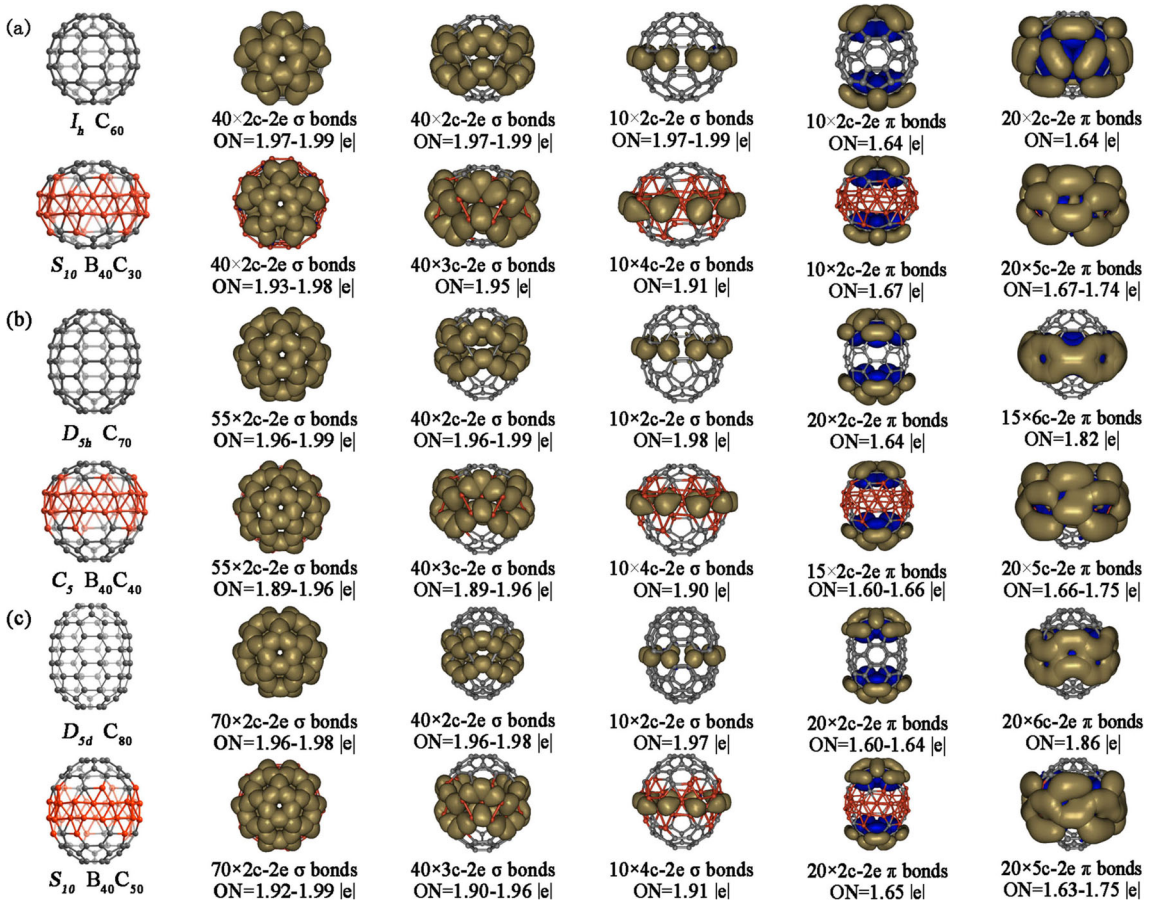

Fig. 3 AdNDP bonding patterns of $B_{40}C_{30}$ (**1**), $B_{40}C_{40}$ (**2**), and $B_{40}C_{50}$ (**3**) in comparison with their carbon fullerene counterparts C_{60}, C_{70}, and C_{80}

has proven to be a powerful means to characterize novel clusters in gas phases [40, 41]. As shown in Fig. 4a and b, $B_{40}C_{30}$ (**1**) possesses six major IR-active peaks at 690, 780, 865, 1043, 1057, and 1272 cm^{-1} and six major Raman-active modes at 193, 317, 972, 1281, 1543, and 1606 cm^{-1}. The Raman vibration at 317 cm^{-1} originates from the typical radial breathing mode (RBM) of the cage-like $B_{40}C_{30}$ (**1**), which can be used to characterize its hollow cage-like structure [42]. The strong UV absorption peaks at 342, 375, and 390 nm mainly originate from electron transitions from the deep inner shells to the high-lying unoccupied molecular orbitals of $B_{40}C_{30}$ (**1**), while the weak absorption bands that occur above 450 nm mainly originate from electron transitions involving the HOMO and its neighboring occupied orbitals.

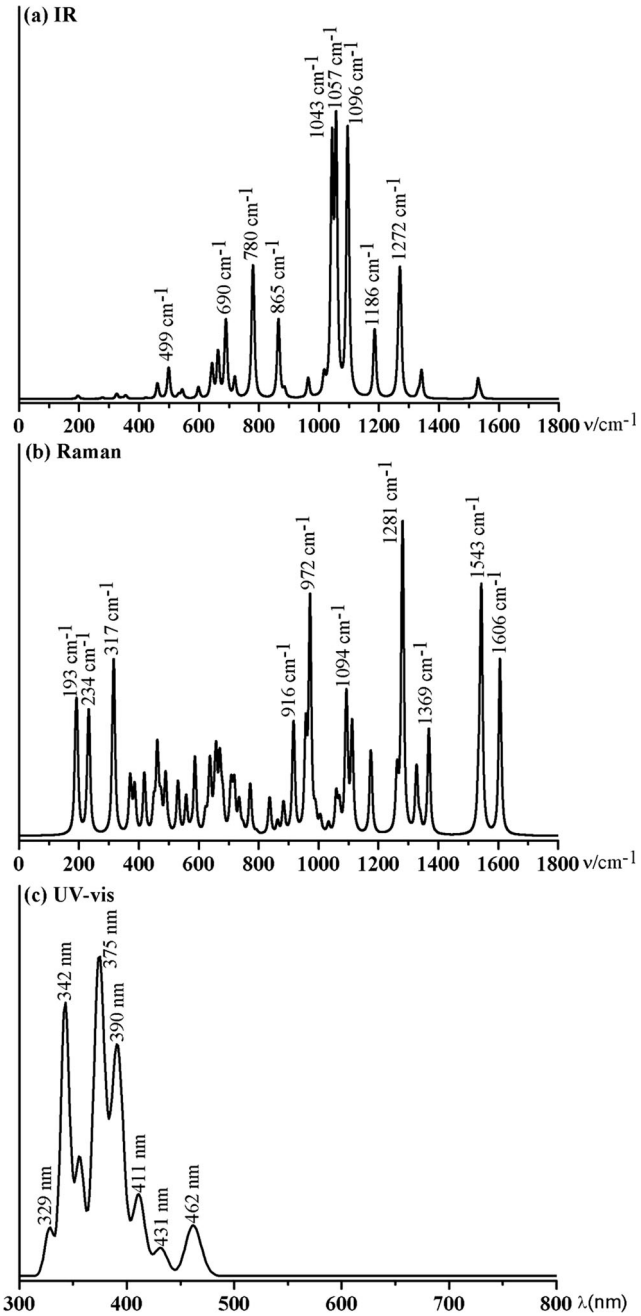

Fig. 4 Simulated IR, Raman, and UV-vis spectra of $B_{40}C_{30}$ (**1**) as calculated at the PBE0/6-31G* level

Conclusions

Based on extensive first-principles theory calculations, we were able to predict the possible existence of the high-symmetry heterofullerenes S_{10} $B_{40}C_{30}$ (**1**), C_5 $B_{40}C_{40}$ (**2**), and S_{10} $B_{40}C_{50}$ (**3**), each of which feature one B_{30} BDC nanoring at the equator, two C_{15} or C_{25} carbon caps at the top and bottom, and ten quasi-planar tetracoordinate C atoms in ten B-centered B_6C hexagonal pyramids around the waist in a seamless patched structural motif, resulting in novel borafullerenes with high boron contents that are isovalent with the typical fullerenes C_{60}, C_{70}, and C_{80}. Detailed orbital and bonding analyses indicate that all three heterofullerenes contain 20 delocalized 5c-2e π-bonds in ten hexagonal pyramids that are evenly distributed around the waist. Such a bonding pattern confers high stability to the heterofullerenes which, with HOMO–LUMO energy gaps of > 2.60 eV, may be synthesized by the laser ablation of mixed C-B targets, arc discharge from mixed C-B electrodes, or the direct exposure of fullerenes to boron vapor via atom exchange [11]. A wide range of B_mC_n heterofullerenes that may conform to the isovalent principle should also be explored in order to bridge the gap between pure borospherenes and carbon fullerenes.

Acknowledgements This work was supported by the National Natural Science Foundation of China (21720102006 to S.-D. Li and U1510103 to X.-X. Tian).

References

1. Kroto HW, Heath JR, O'Brien SC, Curl RF, Smalley RE (1985) C_{60}: buckminsterfullerene. Nature 318:162–163
2. Taylor R, Hare JP, Abdul-Sada AK, Kroto HW (1990) Isolation, separation and characterisation of the fullerenes C_{60} and C_{70}: the third form of carbon. J Chem Soc Chem Commun 22:1423–1425
3. Krätschmer W, Lamb LD, Fostiropoulos K, Huffman DR (1990) Solid C_{60}: a new form of carbon. Nature 347:354–358
4. Rabenau T, Simon A, Kremer RK, Sohmen E (1993) The energy gaps of fullerene C_{60} and C_{70} determined from the temperature dependent microwave conductivity. Z Phys B 90:69–72
5. Guo T, Jin CM, Smalley RE (1991) Doping bucky: formation and properties of boron-doped buckminsterfullerene. J Phys Chem 95: 4948–4950
6. Muhr HJ, Nesper R, Schnyder B, Kötz R (1996) The boron heterofullerenes $C_{59}B$ and $C_{69}B$: generation, extraction, mass spectrometric and XPS characterization. Chem Phys Lett 249:399–405
7. Kurita N, Kobayashi K, Kumahora H, Tago K, Ozawa K (1992) Molecular structures, binding energies and electronic properties of dopyballs $C_{59}X$ (X= B, N and S). Chem Phys Lett 198:95–99

8. Garg I, Sharma H, Dharamvir K, Jindal VK (2011) Substitutional patterns in boron doped heterofullerenes $C_{60-n}B_n$ (n = 1–12). J Comput Theor Nanosci 8:642–655
9. Zhong XL, Pandey R, Rocha AR, Karna SP (2010) Can single-atom change affect electron transport properties of molecular nanostructures such as C_{60} fullerene? J Phys Chem Lett 1:1584–1589
10. Li FY, D-e J, Chen ZF (2014) Computational quest for spherical $C_{12}B_{68}$ fullerenes with "magic" π-electrons and quasi-planar tetracoordinated carbon. J Mol Model 20:2085–2013
11. Mohr S, Pochet P, Amsler M, Schaefer B, Sadeghi A, Genovese L, Goedecker S (2014) Boron aggregation in the ground states of boron-carbon fullerenes. Phys Rev B 89:041404
12. Dunk PW, Rodríguez-Fortea A, Kaiser NK, Shinohara H, Poblet JM, Kroto HW (2013) Formation of heterofullerenes by direct exposure of C_{60} to boron vapor. Angew Chem Int Ed 52:315–319
13. Szwacki GN, Sadrzadeh A, Yakobson BI (2007) B_{80} fullerene: an ab initio prediction of geometry, stability, and electronic structure. Phys Rev Lett 98:166804–166804
14. Prasad DLVK, Jemmis ED (2008) Stuffing improves the stability of fullerenelike boron clusters. Phys Rev Lett 100:165504
15. Li FY, Jin P, D-e J, Wang L, Zhang SB, Zhao JJ, Chen ZF (2012) B_{80} and $B_{101–103}$ clusters: remarkable stability of the core-shell structures established by validated density functionals. J Chem Phys 136:074302
16. Zhai HJ, Zhao YF, Li WL, Chen Q, Bai H, Hu HS, Piazza ZA, Tian WJ, Lu HG, Wu YB, Mu YW, Wei GF, Liu ZP, Li J, Li SD, Wang LS (2014) Observation of an all-boron fullerene. Nat Chem 6:727–731
17. He RX, Zeng XC (2015) Electronic structures and electronic spectra of all-boron fullerene B_{40}. Chem Commun 51:3185–3188
18. Chen Q, Li WL, Zhao YF, Zhang SY, Hu HS, Bai H, Li HR, Tian WJ, Lu HG, Zhai HJ, Li SD, Li J, Wang LS (2015) Experimental and theoretical evidence of an axially chiral borospherene. ACS Nano 9:754–760
19. Chen Q, Zhang SY, Bai H, Tian WJ, Gao T, Li HR, Miao CQ, Mu YW, Lu HG, Zhai HJ, Li SD (2015) Cage-like B_{41}^+ and B_{42}^{2+}: new chiral members of the borospherene family. Angew Chem Int Ed 54:8160–8164
20. Chen Q, Li HR, Miao CQ, Wang YJ, Lu HG, Mu YW, Ren GM, Zhai HJ, Li SD (2016) Endohedral Ca@B_{38}: stabilization of a B_{38}^{2-} borospherene dianion by metal encapsulation. Phys Chem Chem Phys 18:11610–11615
21. Chen Q, Li HR, Tian WJ, Lu HG, Zhai HJ, Li SD (2016) Endohedral charge-transfer complex Ca@B_{37}^-: stabilization of a B_{37}^{3-} borospherene trianion by metal-encapsulation. Phys Chem Chem Phys 18:14186–14190
22. Tian WJ, Chen Q, Li HR, Yan M, Mu YW, Lu HG, Zhai HJ, Li SD (2016) Saturn-like charge-transfer complexes Li_4&B_{36}, Li_5&B_{36}^+, and Li_6&B_{36}^{2+}: exohedral metalloborospherenes with a perfect cage-like B_{36}^{4-} core. Phys Chem Chem Phys 18:9922–9926
23. Wang YJ, Zhao YF, Li WL, Jian T, Chen Q, You XR, Ou T, Zhao XY, Zhai HJ, Li SD, Li J, Wang LS (2016) Observation and characterization of the smallest borospherene, B_{28}^- and B_{28}. J Chem Phys 144:064307
24. Li HR, Jian T, Li WL, Miao CQ, Wang YJ, Chen Q, Luo XM, Wang K, Zhai HJ, Li SD, Wang LS (2016) Competition between quasi-planar and cage-like structures in the B_{29}^- cluster: photoelectron spectroscopy and ab initio calculations. Phys Chem Chem Phys 18:29147–29155
25. Chen X, Zhao YF, Wang LS, Li J (2017) Recent progresses of global minimum searches of nanoclusters with a constrained basin-hopping algorithm in the TGMin program. Comput Theor Chem 1107:57–65
26. Zhao Y, Chen X, Li J (2017) TGMin: a global-minimum structure search program based on a constrained basin-hopping algorithm. Nano Res 10:3407–3420
27. Goedecker S, Hellmann W, Lenosky T (2005) Global minimum determination of the Born–Oppenheimer surface within density functional theory. Phys Rev Lett 95:055501
28. Goedecker S (2004) Minima hopping: an efficient search method for the global minimum of the potential energy surface of complex molecular systems. J Chem Phys 120:9911–9917
29. Adamo C, Barone V (1999) Toward reliable density functional methods without adjustable parameters: the PBE0 model. J Chem Phys 110:6158–6170
30. Krishnan R, Binkley JS, Seeger R, Pople JA (1980) Self-consistent molecular orbital methods. XX. A basis set for correlated wave functions. J Chem Phys 72:650–654
31. Zubarev DY, Boldyrev AI (2009) Deciphering chemical bonding in golden cages. J Phys Chem A 113:866–868
32. Zubarev DY, Boldyrev AI (2008a) Revealing intuitively assessable chemical bonding patterns in organic aromatic molecules via adaptive natural density partitioning. J Org Chem 73:9251–9258
33. Zubarev DY, Boldyrev AI (2008b) Developing paradigms of chemical bonding: adaptive natural density partitioning. Phys Chem Chem Phys 10:5207–5217
34. Varetto U (2009) Molekel 5.4.0.8. Swiss National Supercomputing Center, Manno
35. Frisch MJ, Trucks GW, Schlegel HB, Scuseria GE, Robb MA, Cheeseman JR, Scalmani G, Barone V, Mennucci B, Petersson GA et al (2009) Gaussian 09, revision D.01. Gaussian, Inc., Wallingford
36. Averkiev BB, Wang LM, Huang W, Wang LS, Boldyrev AI (2009) Experimental and theoretical investigations of CB_8^-:towards rational design of hypercoordinated planar chemical species. Phys Chem Chem Phys 11:9840–9849
37. Galeev TR, Li WL, Romanescu C, Cernusak I, Wang LS, Boldyrev AI (2012) Photoelectron spectroscopy and ab initio study of boron-carbon mixed clusters: CB_9^- and $C_2B_8^-$. J Chem Phys 137:234306
38. Reyes HNV, Anota EC, Castro M (2018) C_{60}-like boron carbide and carbon nitride fullerenes: stability and electronic properties obtained by DFT methods. Fuller Nanotub Car N 26:52–60
39. Schleyer PV, Maerker C, Dransfeld A, Jiao HJ, Hommes NJRV (1996) Nucleus-independent chemical shifts: a simple and efficient aromaticity probe. J Am Chem Soc 118:6317–6318
40. Wang GJ, Zhou MF, Goettel JT, Schrobilgen GJ, Su J, Li J, Schlöder T, Riedel S (2014) Identification of an iridium-containing compound with a formal oxidation state of IX. Nature 514:475–477
41. Fagiani MR, Song XW, Petkov P, Debnath S, Gewinner S, Schöllkopf W, Heine T (2017) Untersuchung der struktur und dynamik des B_{13}^+ mithilfe der infrarot-photodissoziationsspektroskopie. Angew Chem 129:515–519
42. Ciuparu D, Klie RF, Zhu YM, Pfefferle L (2004) Synthesis of pure boron single-wall nanotubes. J Phys Chem B 108:3967–3969